DOT/FAA/NR-92/8, I

Program Director for Surveillance
Washington, DC 20591

On the Potential Use of the Terminal Doppler Weather Radar Gust Front Detection Algorithm On the WSR–88D System

Part I: Impacts of Radar System Differences

Gregory J. Stumpf

NOAA/ERL National Severe Storms Laboratory
1313 Halley Circle
Norman, OK 73069

September 1991

Interim Report

U.S. Department of Transportation
Federal Aviation Administration

DISCLAIMER NOTICE

THIS DOCUMENT IS BEST QUALITY AVAILABLE. THE COPY FURNISHED TO DTIC CONTAINED A SIGNIFICANT NUMBER OF COLOR PAGES WHICH DO NOT REPRODUCE LEGIBLY ON BLACK AND WHITE MICROFICHE.

Technical Report Documentation Page

1. Report No.	2. Government Accession No.	3. Recipient's Catalog No.
DOT/FAA/NR-92/8, I		

4. Title and Subtitle	5. Report Date
On the Potential Use of the Terminal Doppler Weather Radar Gust Front Detection Algorithm on the WSR-88D System Part I: Impacts of Radar System Differences	September 1991
	6. Performing Organization Code
	8. Performing Organization Report No.
7. Author(s): Gregory J. Stumpf	
9. Performing Organization Name and Address: NOAA/ERL National Severe Storms Laboratory, 1313 Halley Circle, Norman, OK 73069	10. Work Unit No. (TRAIS)
	11. Contract or Grant No. DTFAO1-80-Y-10524
	13. Type of Report and Period Covered: Interim Report
12. Sponsoring Agency Name and Address: U.S. Department of Transportation, Federal Aviation Administration, 800 Independence Avenue, SW, Washington, DC 20591	14. Sponsoring Agency Code: ANR-150
15. Supplementary Notes	

16. Abstract

The feasibility of using the gust front detection algorithm (GFDA) developed for the Terminal Doppler Weather Radar (TDWR) system on a Next Generation Weather Radar [WSR-88D (formerly NEXRAD)] system is assessed. The data resolution and tilt sequences of the WSR-88D system are different than TDWR, and the WSR-88D is designed to operate at greater ranges. To test the effect of the decreased data resolution of WSR-88D, TDWR-like data were degraded to the resolution of WSR-88D and the GFDA was tested on this degraded dataset. Also, the GFDA was tested on a gust front which occurred outside the normal 60-km range in which data are processed for TDWR. Results show that the degraded velocity precision of WSR-88D has little effect on the performance of the GFDA. However, the larger sample volume sizes for the WSR-88D system did degrade the performance of the GFDA. The second lowest tilt angle for the WSR-88D tilt sequences is about 0.5° higher than TDWR, and this reduced the maximum range of gust front detectability. These tests show that the GFDA's performance on the WSR-88D system will be acceptable after a few modifications.

17. Key Words	18. Distribution Statement
Doppler Radar, Algorithm, Aviation, Gust Front, Wind Shift, WSR-88D, TDWR	This document is available to the public through the National Technical Information Service, Springfield, VA 22161

19. Security Classif. (of this report)	20. Security Classif. (of this page)	21. No. of Pages	22. Price
Unclassified	Unclassified	39	

Form DOT F 1700.7 (8-72) Reproduction of completed page authorized

ACKNOWLEDGMENTS

The author thanks Mike Eilts, Laurie Hermes, Diana Klingle-Wilson, Don Burgess, Dr. Dusan Zrnić, Kevin Thomas, DeWayne Mitchell, and Mike Jain for their help and valuable comments. Joan Kimpel drafted Fig. 1. Doppler data used in this report were provided by the MIT Lincoln Laboratory under sponsorship from the Federal Aviation Administration. Data were also provided by the National Severe Storms Laboratory.

TABLE OF CONTENTS

LIST OF FIGURES

LIST OF TABLES

ACRONYMS

AWS	Air Force Air Weather Service
FAA	Federal Aviation Administration
FL-2	10-cm Doppler radar operated by MIT/LL
GFDA	Gust Front Detection Algorithm
LL	Lincoln Laboratory
MIT	Massachusetts Institute of Technology
NSSL	National Severe Storms Laboratory
NWS	National Weather Service
OT&E	Operational Test and Evaluation
SAM	Surface Automated Mesonet
TDWR	Terminal Doppler Weather Radar
UTC	Universal Coordinated Time
VCP	Volume Coverage Pattern
WSR-88D	Next Generation Weather Radar (formerly NEXRAD)

1. Introduction.

A gust front is the leading edge of the cold air outflow originating from thunderstorm downdrafts. Changes in wind speed and direction found along these boundaries can produce wind shears and turbulence severe enough to be hazardous to aircraft during takeoff and landing. These wind shifts also impact runway traffic management.

A Gust Front Detection Algorithm (GFDA) has been developed for the Federal Aviation Administration's (FAA) Terminal Doppler Weather Radar (TDWR) program. By detecting the current location of gust fronts, landing and departing aircraft can be forewarned of these dangerous wind shear conditions. The GFDA also estimates the wind speed and direction on both sides of the gust front[1], and forecasts front positions 10 and 20 minutes into the future. This gives air traffic controller supervisors ample time to plan runway changes without significantly affecting airport operations, reducing the excess fuel consumption caused by unanticipated runway reconfigurations.

In the 1990s, the existing network of antiquated WSR-57 radars in the United States will be replaced by a network of Doppler radars known as Next Generation Weather Radars [WSR-88D (formerly termed NEXRAD)]. This report presents the results of a study that determine potential changes in GFDA performance on the WSR-88D system. This report will also examine what algorithm changes will be

[1]The FAA currently refers to the wind estimation technique as the Wind Shift Algorithm.

needed to allow the GFDA to be added to the suite of computer-based weather detection algorithms being developed for the WSR-88D system.

The WSR-88D users will include the FAA, the National Weather Service (NWS), the United States Air Force's Air Weather Service (AWS), and private industry. Potential uses by these organizations include military air-traffic control by the AWS and in-route air-traffic planning by the FAA. The NWS could use the GFDA for a variety of reasons. These include alerting the public, general aviation, and marine interests of dangerous changes in wind direction and speed. As a severe storms nowcasting tool, the Gust Front Detection Algorithm could be tuned to detect the clear air boundaries which are common foci for convective initiation (Purdom, 1982). Furthermore, products from the GFDA could be assimilated with satellite and mesonetwork data in a nowcast workstation environment.

The scanning strategy of the TDWR system has been designed for the detection of aviation hazards (Campbell and Merritt, 1990). The present GFDA design is based on this scan strategy. The WSR-88D employs several scan strategies and volume coverage patterns which differ from TDWR. Also, the WSR-88D system has a different data resolution than TDWR. These differences, summarized in this report, will affect the performance of the GFDA. Furthermore, the Gust Front Detection Algorithm is designed to detect gust fronts out to a maximum range of 60 km, and WSR-88D users may want to detect gust fronts beyond that range. A discussion is included in this report which highlights what parameters impact the detection of gust fronts at distant ranges.

2. The Gust Front Detection Algorithm.

2.1 Background.

The initial development of the GFDA began in the early 1980's at the National Severe Storms Laboratory (NSSL; Uyeda and Zrnić, 1985). Since then, several upgrades to algorithm techniques have been made (Witt and Smith, 1987; Witt et al., 1989; Hermes et al., 1990).

The algorithm relies on identifying the main attribute which gust fronts possess in Doppler velocity fields, i.e., lines of radial convergence. An Advanced Gust Front Detection Algorithm (AGFDA; Eilts et al., 1991), currently under development, includes azimuthal shear and reflectivity thin line recognition capability to improve gust front detectability. This report focuses on only the radial convergence algorithm, the GFDA. Section 2.2 will briefly describe the techniques used to detect the radial convergent portion of gust fronts, giving emphasis to those portions of the algorithm that will be examined further in Sections 4 and 5 of this report. The reader is asked to refer to Witt et al. (1989) for a more comprehensive description of the GFDA.

2.2 Gust front detection techniques.

The GFDA uses velocity data from two low-altitude elevation scans (0.5° and 1.0°). The algorithm builds radially convergent *shear segments* from smoothed and

dealiased velocity data. These shear segments consist of runs of decreasing radial velocity. As each shear segment is built, several attributes of the segment are compared to minimum thresholds. Thresholded are the *velocity difference* between the beginning and ending velocities of the segment (Δv), and the maximum velocity difference computed over a ≈1 km distance within the segment (called *peak shear*). Typical threshold settings (used during real-time testing at Denver Colorado in 1988) are $\Delta v = 7$ m s^{-1} for the 0.5° tilt, $\Delta v = 5$ m s^{-1} for the 1.0° tilt, and peak shear = 2 m s^{-1} km^{-1} for both tilt angles. These thresholds have been chosen empirically to increase probability of gust front detection while reducing the number of false alarms. The *peak shear location* is defined by the slant range to the center of the 1 km window over which the peak shear is calculated.

Individual shear segments are combined into *shear features* based on spatial proximity. Shear segments are placed into a common feature if their peak shear locations are separated by no more than 2.2° in azimuth and 2 km in range. If there are fewer than five segments in the feature, that feature is discarded. Two features from the same elevation scan are combined if the end points of the features are within 5 km of each other. Shear features from the two low-altitude scans are *vertically associated* to declare *gust front detections*, and the peak shear locations are represented as a smooth curve.

If one or more gust fronts are detected on two consecutive radar volume scans, an attempt is made to establish time continuity between fronts. If a front has been time associated, 10 and 20 minute forecast positions are produced by the

algorithm, and an attempt is made to estimate the horizontal wind speed and direction on both sides of the gust front. Finally, an estimate of the wind shear that an aircraft might experience upon encountering a gust front (wind shear hazard) is computed. This estimate is the sum of the mean plus one standard deviation of every peak shear values for each shear feature used in making a gust front detection.

3. WSR-88D and TDWR Operational Modes.

Table 1 compares several attributes of the TDWR Hazardous Weather Mode scan strategy (Campbell and Merritt, 1990) with the WSR-88D scan strategies (U. S. Dept. of Commerce, 1988). Only the two low-altitude tilts used by the GFDA are included for brevity[2].

The WSR-88D system uses scan strategies and volume coverage patterns (VCP) that differ from TDWR. Presently, the WSR-88D operates using a choice of two operational modes, the precipitation mode and the clear-air mode. Three scan strategies have been specified with provisions included for later expansion to as many as eight (Heiss et al., 1990). Two of the scan strategies are used when operating in the precipitation mode. Both strategies use a short pulse width providing a gate spacing of 250 m. The third scan strategy is used during clear-air operations and consists of two VCPs. One clear-air VCP uses a short pulse width providing a gate spacing of 250 m. The other uses a long pulse, providing a 750 m gate spacing, but

[2]These are the scan strategies used as of March 1990, and are subject to change (Sirmans, personal communication).

increases the system sensitivity by 8 dB. Each scan strategy has a choice of velocity precisions, either 0.5 m s^{-1} (the normal setting), or 1.0 m s^{-1}.

Table 1. Some system differences between TDWR and WSR-88D. "P" and "C" denote the "precipitation" and "clear-air" operating modes respectively.

RADAR SYSTEM	OPER MODE	PULSE WIDTH MODE	1st TILT ANGLE	2nd TILT ANGLE	GATE SPACING (m)
TDWR	P	Short	0.50°	1.00°	120
WSR-88D	P	Short	0.50°	1.45°	250
WSR-88D	P	Short	0.40°	1.35°	250
WSR-88D	C	Short	0.50°	1.50°	250
WSR-88D	C	Long	0.50°	1.50°	750

TYPE OF RADAR	OPER MODE	PULSE WIDTH MODE	GATE SIZE (m)	SCAN RATE (s)	VELOCITY PRECISION (m/s)
TDWR	P	Short	100	300	0.01
WSR-88D	P	Short	250	300	0.5 or 1.0
WSR-88D	P	Short	250	360	0.5 or 1.0
WSR-88D	C	Short	250	600	0.5 or 1.0
WSR-88D	C	Long	750	600	0.5 or 1.0

The TDWR Hazardous Weather Mode, a precipitation mode, has a data resolution of 120 m gate spacing and a 0.01 m s^{-1} velocity precision. The two low-elevation tilt angles are 0.5° and 1.0°, and the scan update rate is 5 minutes[3].

In summary, WSR-88D's second low-elevation tilt angle can be as much as 0.5° higher than TDWR's. The radar sample volume (gate) spacing and size are about doubled. Also, the velocity precision is degraded on the WSR-88D system. Scan

[3]TDWR also has a clear-air mode called the Monitor Mode (Campbell and Merritt, 1990). This mode is used when no significant weather returns are present within 30 km of the radar site. The GFDA only operates when the radar is in the Hazardous Weather Mode.

update time varies for each of the WSR-88D strategies. Otherwise, WSR-88D system characteristics are similar to TDWR.

4. Impacts of Data Resolution and Velocity Precision Differences.

4.1 Test Methodology.

Twenty sample scans of Doppler velocity data were used to test the effects of the gate spacing and velocity precision differences between the two radar systems, on the GFDA. These radar data were collected by the Massachusetts Institute of Technology/Lincoln Laboratory (MIT/LL) FL-2 testbed Doppler radar in Denver, Colorado on 22 June 1988 using a TDWR scan strategy. To create a simulated WSR-88D data set, the TDWR-like data were degraded by removing every other range gate, giving a spacing of 240 m. Also, the velocity precision at each gate was reduced to 0.5 m s^{-1} (1.0 m s^{-1} precision was not tested).

The algorithm was run on every scan using both the original TDWR-like data set and the simulated WSR-88D data set. Tests were also run to determine the individual effects of gate spacing and velocity precision. This was done by creating two more data sets, one that had only the gate spacing degradation, and another data set that had only the velocity precision degradation.

4.2 Test Results.

Table 2 shows the impact of these tests during the shear segment building phase of the algorithm. Using the original TDWR-like data set, the GFDA detected 5412 shear segments. The change in velocity precision had very little effect. Also, average Δv values are basically unaffected by these radar system differences. However, the gate spacing differences had a significant effect. The average length of shear segments was about 33% greater when the gate spacing was 240 m. Also, average peak shear values were about 33% smaller and there was a 22% reduction in the number of shear segments produced.

Table 2. Results of testing different gate size and velocity precisions on 20 tilts of data collected at Denver CO, on 22 June 88.

GATE SIZE (m)	VELOCITY PRECISION (m/s)	NUMBER OF SHEAR SEGMENTS	AVERAGE SEGMENT LENGTH (m)	AVERAGE VELOCITY DIFFERENCE (m/s)	AVERAGE PEAK SHEAR (m/s/km)
120	0.01	5412	4.61	8.27	5.65
240	0.01	4176	6.07	8.39	3.75
120	0.5	5422	4.70	8.23	5.59
240	0.5	4202	6.16	8.32	3.72

Peak shear is calculated by finding the largest velocity difference between the first and last sample volumes of a window roughly 1 km long within a shear segment. The algorithm specifies the window size depending upon the resolution of the data. For gate spacing less than 200 m, this peak shear window is 7 gates across. When the gate spacing is greater than 200 m, this peak shear window is 5 gates across. For

example, a 240 m gate spacing gives windows which are 1200 m long, and a 120 m gate spacing gives 840 m long windows, about 30% smaller than the 240 m gate spacing. This 30% reduction in the window size in which peak shear is calculated corresponds roughly to a 33% reduction of average peak shear values when using a 240 m gate spacing (Table 2). Additionally, the reduction in peak shear magnitude is reflected as a 35% reduction in wind shear hazard values (Klingle-Wilson, personal communication).

The WSR-88D long pulse width clear-air mode uses a sample resolution of 750 m, about 6 times larger than TDWR. In this case, the windows across which peak shear is calculated will be 5 gates across and 3.75 km long. Although tests were not performed to evaluate the impact of 750 m resolution, a further degradation of algorithm performance is expected.

Radial convergence must occur over a larger distance using a 240 m gate spacing for a shear segment to be identified (1200 m versus 840 m). Therefore, fewer shear segments will be built. This leads to the increase in average segment length and the decrease in the number of shear segments built at the larger gate spacing.

How do these degradations impact the overall performance of the GFDA? Using a similar set of degraded radar data, Klingle-Wilson (personal communication) determined the impact of a WSR-88D gate size and velocity precision on the algorithm's overall performance. There was a decrease in the Probability of Detection (number of detected events per number of all events) of gust fronts by 7%. Additionally, the average Percent of Length Detected (length of gust front detected

divided by the total true length of a gust front) decreased by 6%. The Probability of False Alarm (number of false alarms per number of correct plus false alarms) increased by 0.6%.

4.3 Possible Solutions.

The algorithm procedure used to calculate the peak shear window sizes could be modified to alleviate these problems. The algorithm could be changed to compute the number of gates which creates a window size which is nearest to 1 km. For example, given a 240 m gate spacing, the window length should be only 4 gates long (or 960 m) instead of 5 gates. The peak shear location would remain as the midpoint of these windows.

5. Scan Strategy Update Rate Comparisons.

The maximum difference between the TDWR and WSR-88D scan strategy update rate is with the clear-air/long pulse width WSR-88D scan strategy (10 minutes versus 5 minutes for TDWR). Significant algorithm performance degradation should only in general be limited to this mode, and should only be significant in a small percentage of cases. The other WSR-88D modes (precipitation) have 5- and 6-minute update rates, thus little effect on algorithm performance is expected in these modes.

Often, gust front orientation, shape, and associated signal return can change significantly between scans that are more than 5 minutes apart. For rapidly evolving gust fronts, significant variations in gust front detections can occur. This can have a significant effect on determining time association of gust fronts. These variations amplify as the scan update rate is lengthened.

As a test, the GFDA was run on two cases, June 22, 1988, and July 16, 1988 [data were collected in Denver CO in support of the TDWR OT&E (Operational Test and Evaluation) on MIT/LL's FL-2 testbed Doppler radar]. One set of tests ran the algorithm on the original data containing a 5-minute scan update rate. The second set of tests was run on data which had every other scan removed, effectively creating a 10-minute scan update rate.

There were 31 instances from both days where gust fronts were detected on three consecutive 5-minute scans. In these instances, the differences were compared between forecasts made by time associating the current fronts with fronts 5 and 10 minutes previous respectively. Of these 31 examples, there were only 3 cases where the two sets of forecasts were more than 2 km in difference. All 3 cases were examples of gust fronts whose detections changed significantly over the 10-minute period. The majority of cases showed insignificant differences. Therefore, the scan strategy update rate differences will have a small impact.

6. Detecting Distant or Shallow Gust Fronts.

6.1 Introduction.

Because the siting of TDWR radars will be about 15-30 km from airport runways, the TDWR GFDA has been designed to detect gust fronts only to a maximum range of 60 km. The two low-altitude tilt angles of 0.5° and 1.0° were chosen to detect most gust fronts within this 60 km range. For shallow gust fronts, and for gust fronts at far ranges (beyond 60 km), detectability will be degraded since the center of the radar beam from the upper or both the upper and lower tilts may be well above the area of convergence associated with the gust front.

The height of the radar beam above ground level is determined by several factors. First, the surface of the earth curves away from the beam. Second, the beam's tilt angle will also add to the beam height above the ground. Finally, during normal conditions, atmospheric refraction will cause the beam to curve slightly downwards, but at a radius of curvature less than the earth's curvature[4].

The height (h) of the radar beam above the ground as a function of slant range (r) under normal atmospheric conditions is given by the following equation (Doviak and Zrnić, 1984),

$$h = [r^2 + (k_e a)^2 + 2rk_e a\sin\theta_e]^{1/2} - k_e a \ , \qquad (1)$$

[4]During atmospheric inversion conditions, the radar beam may actually curve enough to intersect the ground, causing echoes of the ground to be shown on the radar screen.

where the earth's radius a = 6340 km, and k_e = 4/3. If h is the average depth of a gust front, and θ_e is the beam tilt angle, then r is the approximate maximum range at which one can expect to detect a gust front.

Gust front depths vary in different environments. For example, using Doppler radar data, Wakimoto (1982) found depths averaging about 2.0 km for Midwest gust fronts near Chicago IL. Mahoney (1988) discovered an average depth of 1.3 km for High Plains gust fronts near Denver CO. Table 3 tabulates the maximum ranges (r) using Eq. (1) for each tilt angle given in Table 1 assuming these two average gust front depths, 1.3 and 2.0 km.

Table 3. The maximum detectable range of gust fronts with depths of 1.3 and 2.0 km using the radar beam angles listed in Table 1.

RADAR SYSTEM	ELEV ANGLE	MAXIMUM RANGE OF DETECTABILITY FOR A GUST FRONT WITH DEPTH OF	
		1.3 km	2.0 km
TDWR	0.5° 1.0°	92 km 62 km	125 km 88 km
WSR-88D	0.4° 0.5° 1.35° 1.45° 1.5°	101 km 92 km 49 km 46 km 45 km	134 km 125 km 71 km 68 km 66 km

Since features must be vertically associated from both the 0.5° tilt and the next higher tilt (about 1.5°) to be detected as fronts in the GFDA, fewer distant fronts and shallow fronts will be detected using a WSR-88D scan strategy. For example, with a 1.5° upper angle, the average High Plains gust front should only be detectable

within 45 km of the radar. The higher second tilt on the WSR-88D will cause some serious negative effects on detecting distant or shallow gust fronts.

Another problem with detecting distant or shallow gust fronts is portrayed in Fig. 1. This figure shows a cross-section of the shear regions delineating updraft and downdraft air motions within a thunderstorm. Drawn on the figure are typical radar beam paths that might be found at a large distance from the radar. Note that as distance increase behind the surface wind shift (where the shear zone contacts the ground), the shear zone becomes more sloped with respect to the ground. The shear zone can eventually become highly sloped as it becomes the interface between the updraft and downdraft portions of a thunderstorm. At far ranges, convergence can be detected along the elevated shear zone behind the gust front, which is actually behind the surface wind shift (beam path "B"). Furthermore, if the two low-elevation angle beam paths intersect the sloped portion of the elevated shear zone a few kilometers behind the surface wind shift, the location of the shear from each tilt might be offset by several kilometers. This could result in a missed vertical association of features between tilts from the same radar scan.

Although Fig. 1 shows one typical thunderstorm cross-section, it should be noted that gust fronts vary in depth and also vary in their distance from the precipitation cores of the thunderstorms. In many cases, as gust fronts mature, they will become more shallow and propagate away from the precipitation cores (Wakimoto, 1982). All these factors must be considered by the algorithm user when detecting distant and shallow gust fronts.

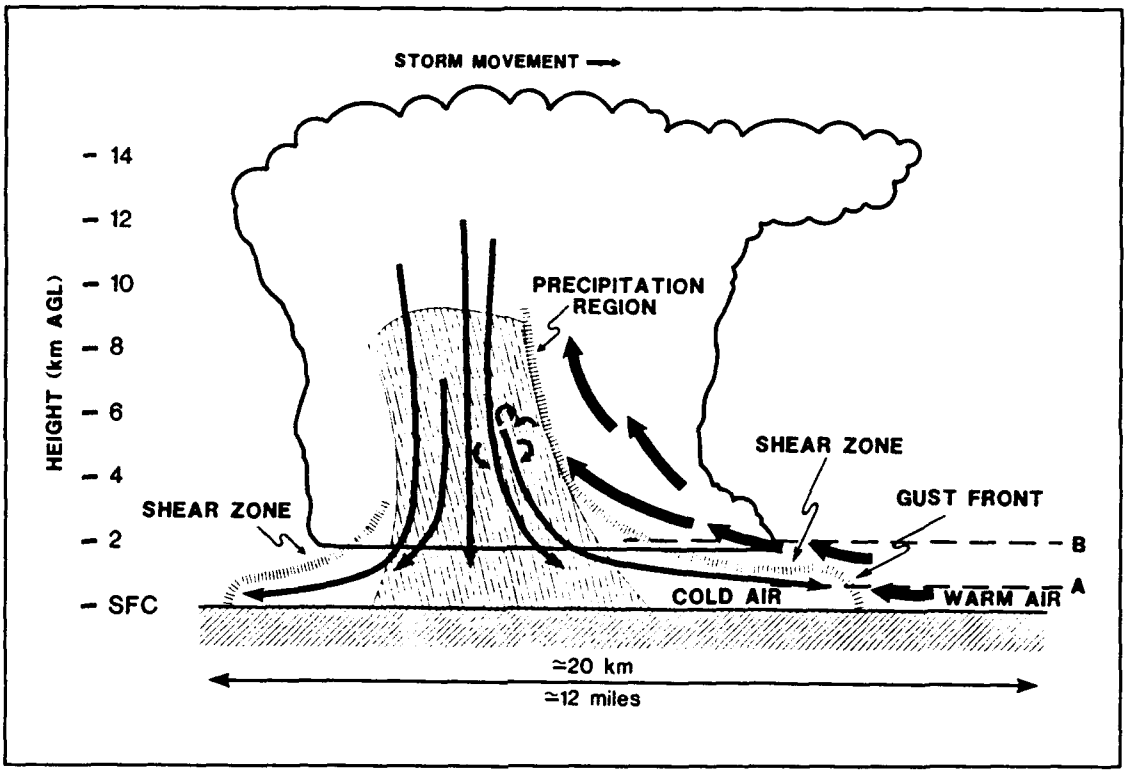

Fig. 1. Vertical cross-section schematic of a typical thunderstorm. Arrows depict airflow. Gray shaded region depicts wind shear zone. Dashed straight lines depict the height of example radar beam paths for different ranges from the radar (i.e., the higher path "B" is for a storm at a farther range than the lower Path "A").

6.2 The 26 April 1984 Case.

The case of 26 April 1984 in Central Oklahoma is presented in this report to highlight some of the intricacies of detecting distant gust fronts. Although the actual surface location of the gust front is known through only several observations from Surface Automated Mesonet (SAM) meteorological observing platforms, some of the observations suggest that this case could be very similar to the schematic presented in Fig. 1.

During the evening of 26 April 1984, a squall line with an accompanying gust front moved across Central Oklahoma. Doppler velocity data were collected with the NSSL Doppler radar located in Norman OK for about 5 hours during the passage of the squall line. The two low-elevation angles of the tilt sequence were set at 0.5° and 1.5°. Between 0134 and 0310 UTC (27 April), the squall line began northwest of the radar and moved southeastward starting from a range of 100 km and ending at 19 km. The GFDA was run on several Doppler radar scans during these times. Table 4 summarizes the gust front detections for the squall line data set.

Table 4. Summary of gust front detections for 26 April 1984.

SCAN TIME (UTC)	FRONT LENGTH (km)	CENTROID AZM (deg)	CENTROID RANGE (km)	WIND ESTIMATES SPEED AHEAD (m/s)	WIND ESTIMATES DIR AHEAD (deg)	WIND ESTIMATES SPEED BEHIND (m/s)	WIND ESTIMATES DIR BEHIND (deg)
0134	59	298°	101	No estimates (first scan)			
0142	74	297°	97	---	----	-----	----
0151	86	300°	87	36	190°	16	255°
0221	94	303°	60	20	178°	15	290°
0228	94	298°	54	29	185°	14	294°
0242	68	309°	38	26	180°	16	273°
0252	86	301°	33	20	174°	17	268°
0302	33	276°	28	14	167°	20	270°
0310	29	273°	19	10	173°	17	273°

Figures 2(a-c) are the 0.5° radial velocity field, the 0.5° reflectivity field, and the shear features and gust front detections respectively at 0134 UTC. The gust front detection is 101 km from the radar. Using Eq. (1), at this range, the 0.5° and the 1.5° beams were 1.5 km and 3.3 km above the earth's surface respectively. The gust front detection is found near the leading edge of a strong reflectivity gradient (Fig. 2b; the

actual location of the surface gust front is unknown). The 1.5° feature (in light blue) for the most part is detected about 3-5 km behind the 0.5° feature (Fig. 2c). The offset between features on the two tilts may be attributed to a sloping gust front interface (Fig. 1).

At 0221 UTC, the gust front detection was located 60 km from the radar (Fig. 3a). At this range, the 0.5° and the 1.5° beams were 0.7 km and 1.8 km above the earth's surface respectively. Along the northern half of the gust front, the distance between the leading edge of the reflectivity gradient and the detection has increased (Fig. 3b). The distance between the 1.5° shear features and the 0.5° features varied along the front (Fig. 3c). Along the northern third of the gust front detection, two 1.5° shear features were roughly on top of the 0.5° shear feature. Along the southern two-thirds of the gust front detection, 1.5° shear features were detected anywhere between 1 and 10 km behind a 0.5° feature.

Superimposed onto Fig. 3a are the locations of two SAM stations (COG and ESW). Within 2 minutes of the radar scan time, the surface gust front passage[5] was recorded at both of these stations. At the same time, the gust front was detected by the GFDA about 5-7 km behind the two SAMs.

[5]At 1 minute intervals, SAMs report the average wind over the previous one minute period. These winds were converted to radial velocities with respect to the Norman radar. The gust front passage time was taken to be the middle time of a run in decreasing radial velocities ("runs" were usually 5-6 minutes long). Gust front passages actually occurred within 1-2 minutes time of the radar scan time. Given an average propagation speed of the gust front of about 14 m s^{-1}, the distance between the SAMs and the gust front detections may be in error by ±1.8 km.

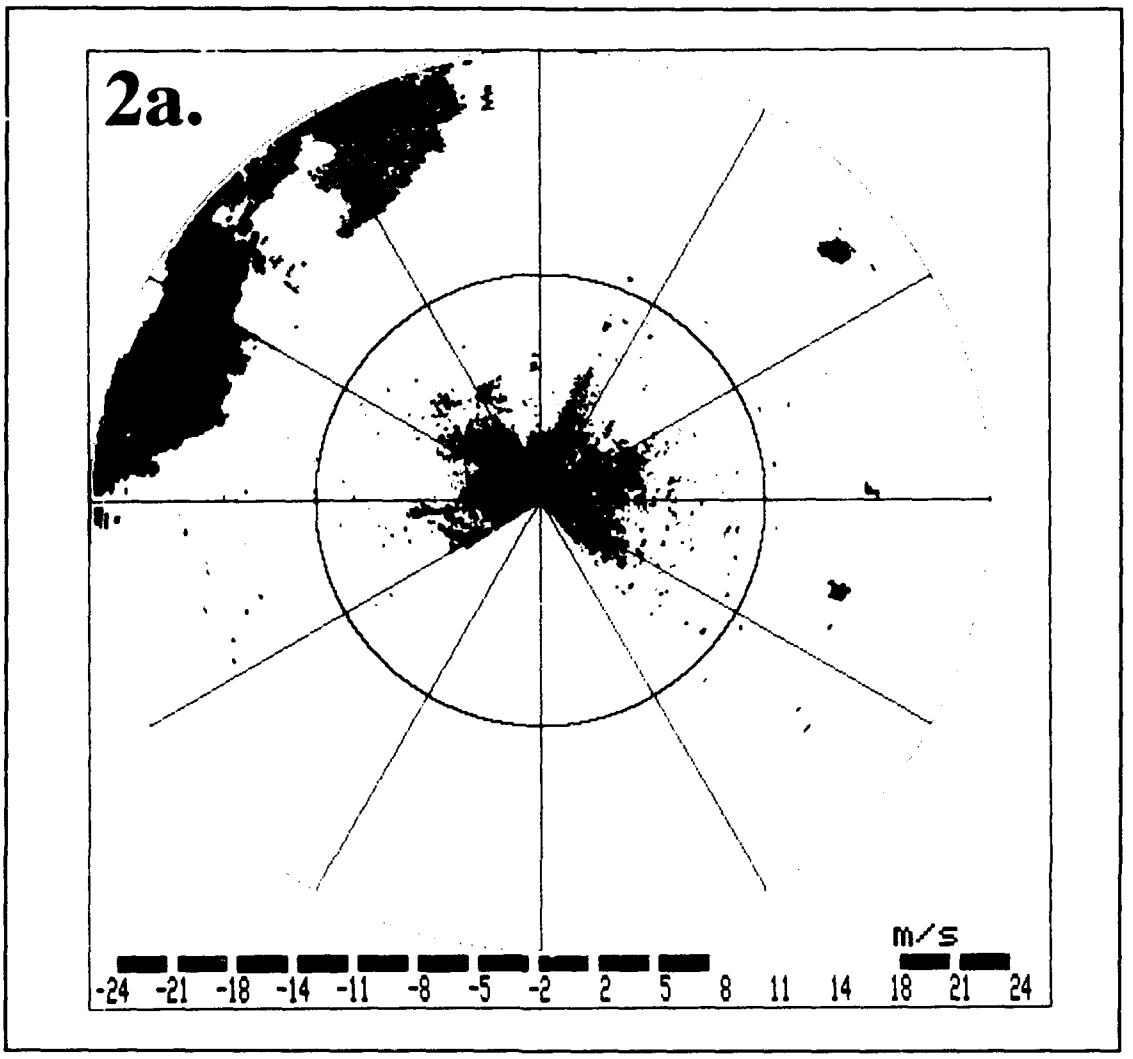

Fig. 2. Data from the NSSL Norman Doppler radar: a) Radial velocity for the 0.5° tilt with gust front detection in red. Positive (negative) velocity values (in m s^{-1}) represent velocities away (toward) the radar; b) reflectivity (dBZ) for the 0.5° tilt with front detections in light blue; c) the 0.5° tilt shear features (in dark blue), the 1.5° tilt shear features (in light blue), and gust front detection (in magenta), at 0134 UTC, 27 April 1984. Range rings are every 60 km.

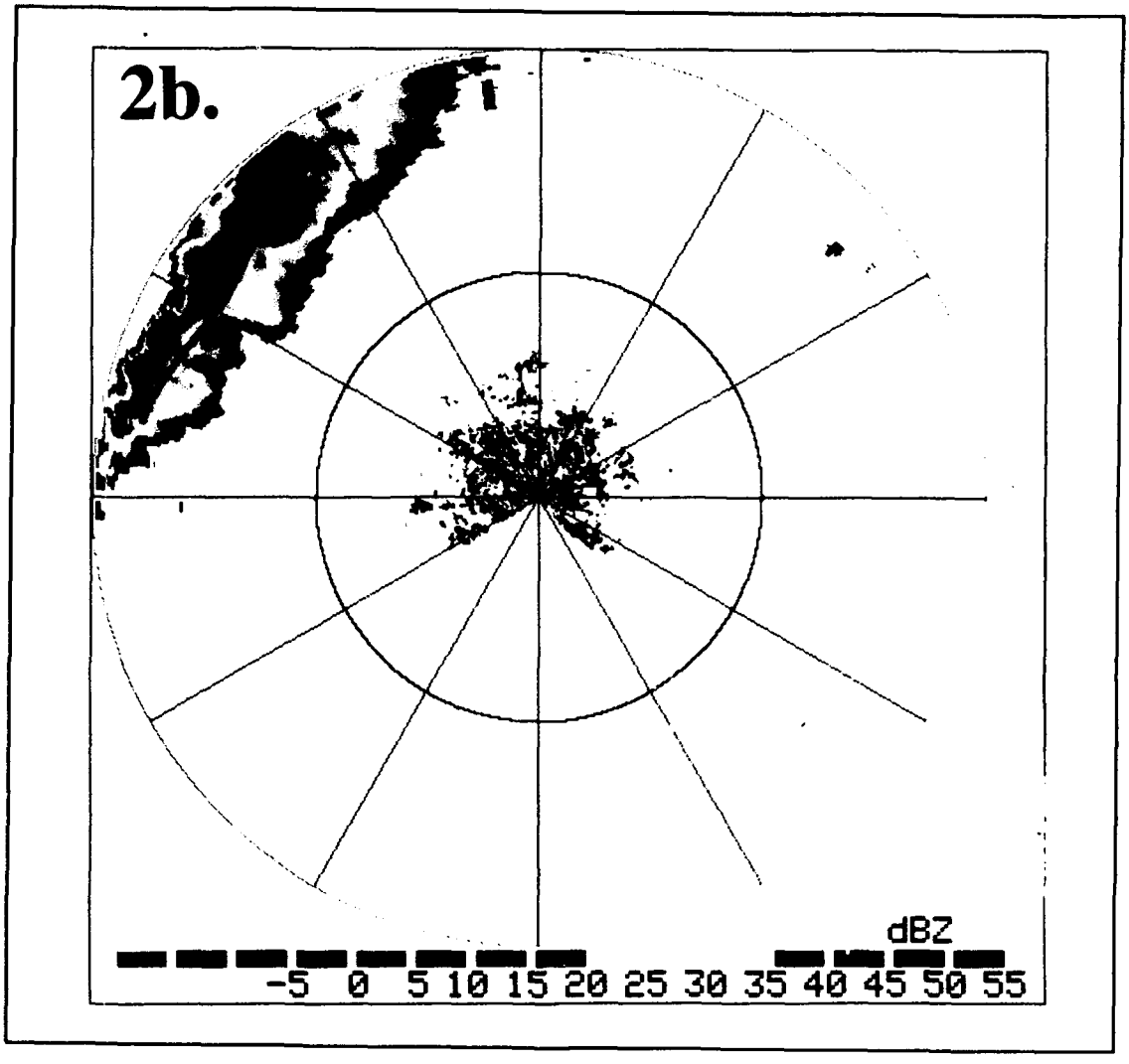

Fig. 2. (continued)

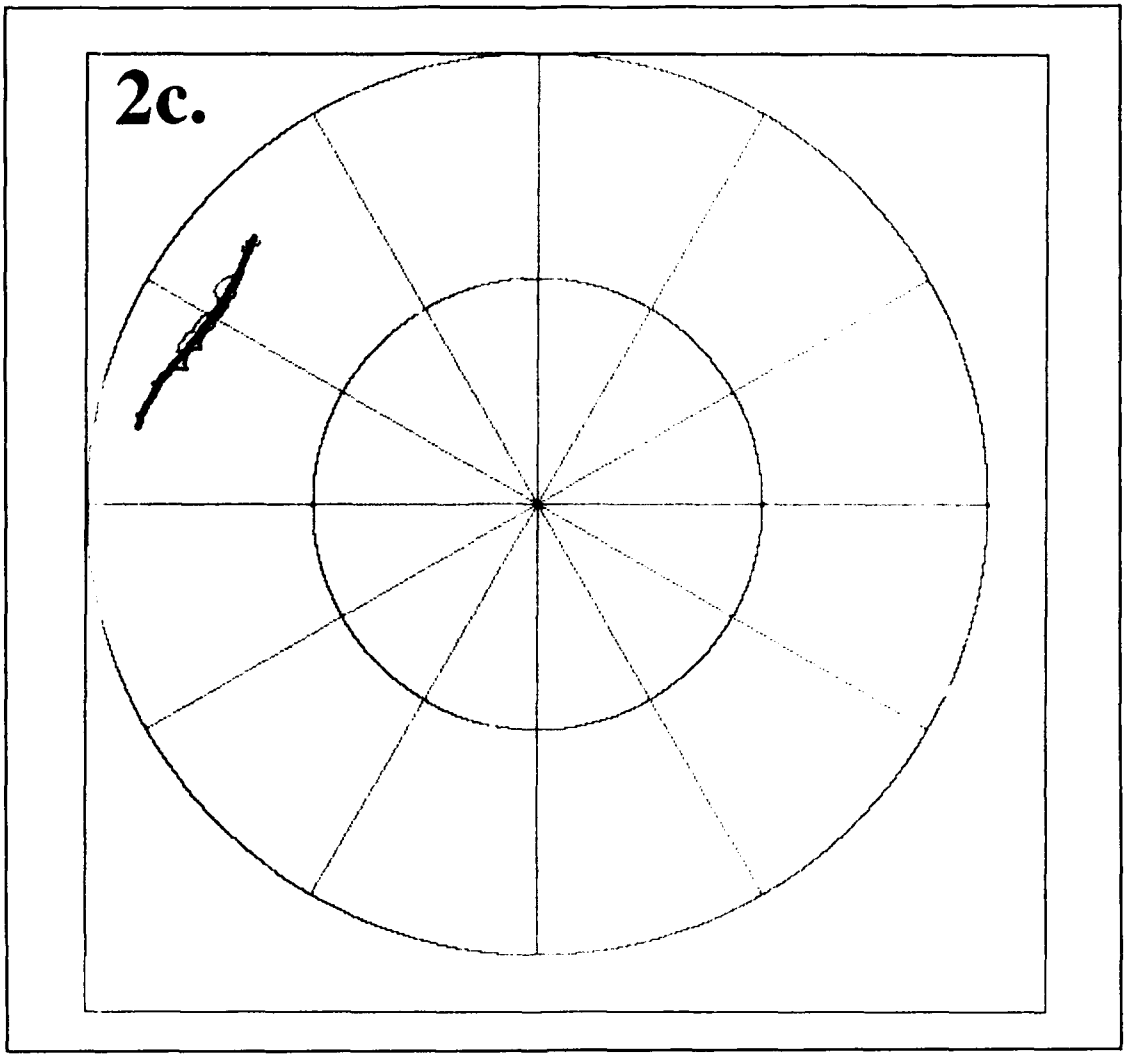

Fig. 2. (continued)

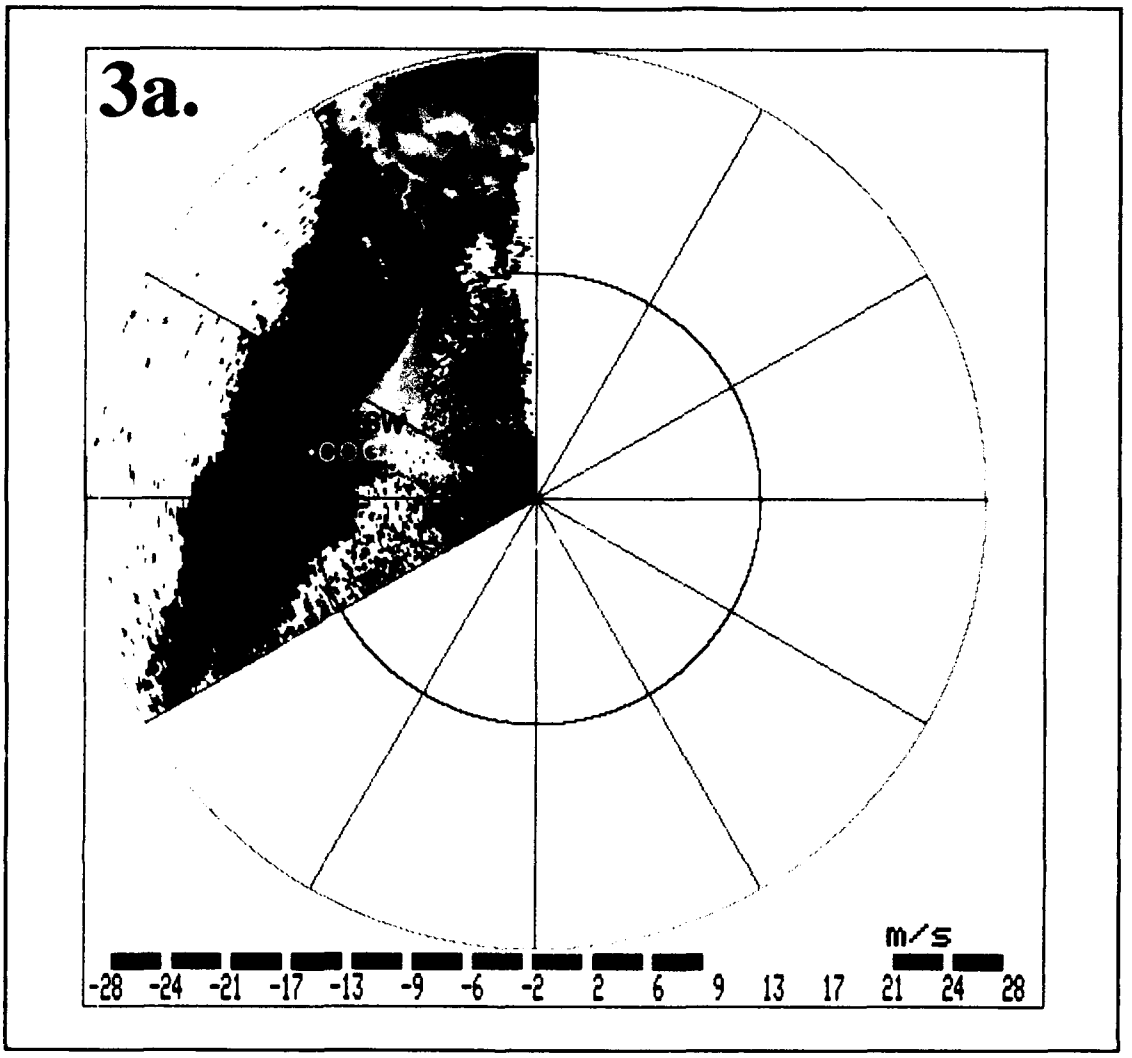

Fig. 3. Same as Fig. 2 except for 0221 UTC. SAM sites ESW and COG measured a surface gust front passage within 2 minutes of this scan. SAM locations are plotted on Fig. 3a.

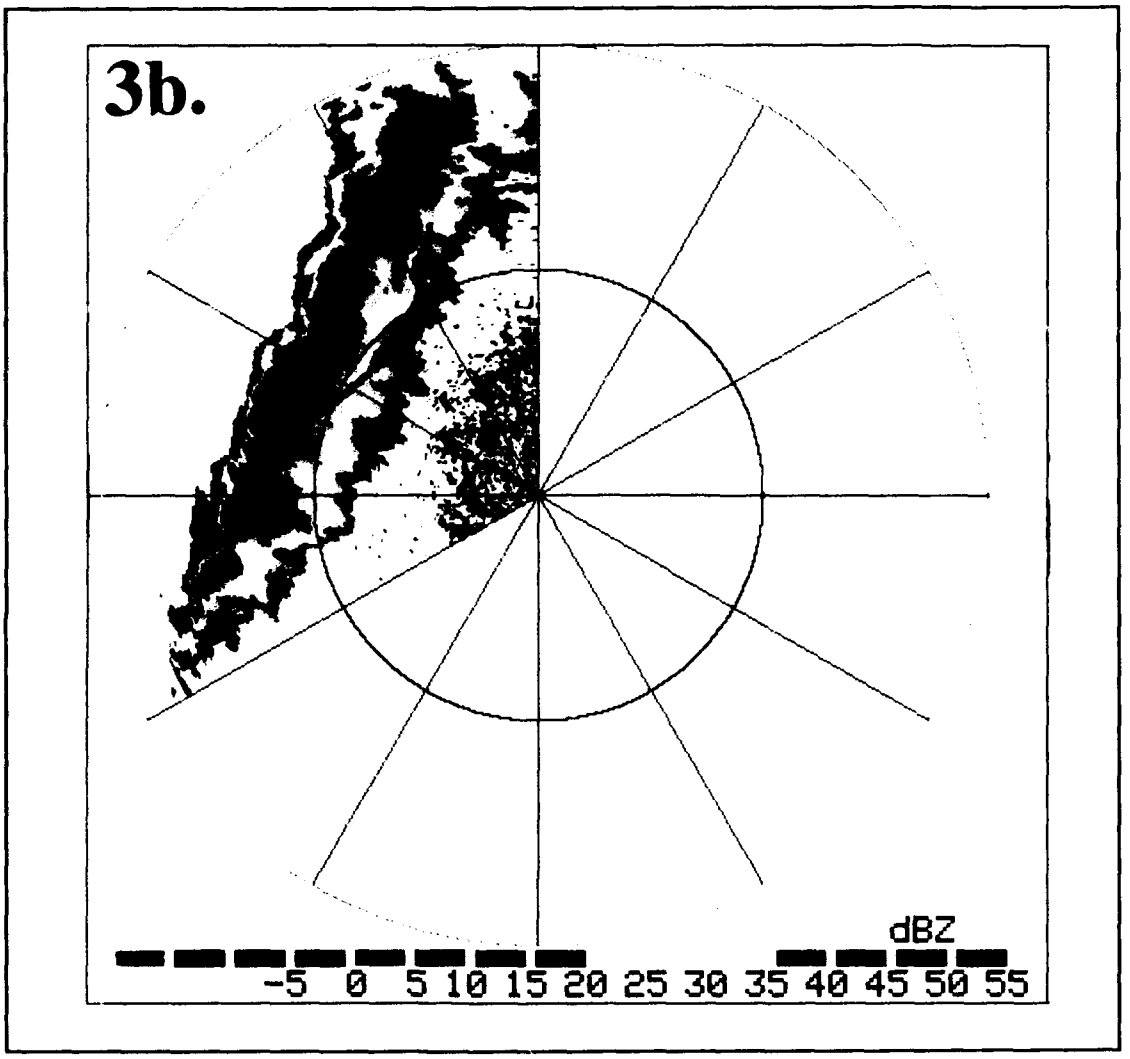

Fig. 3. (continued)

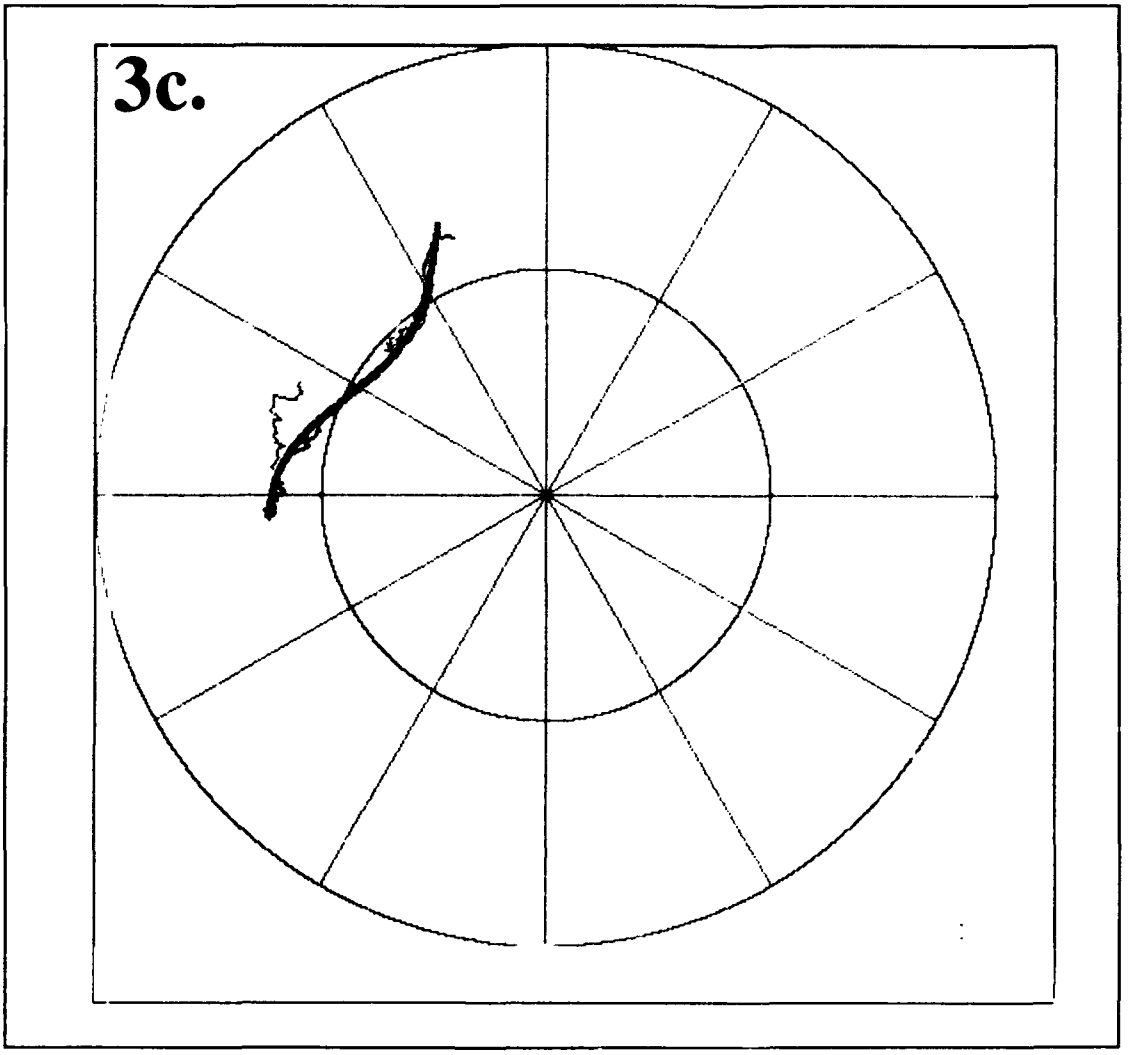

Fig. 3. (continued)

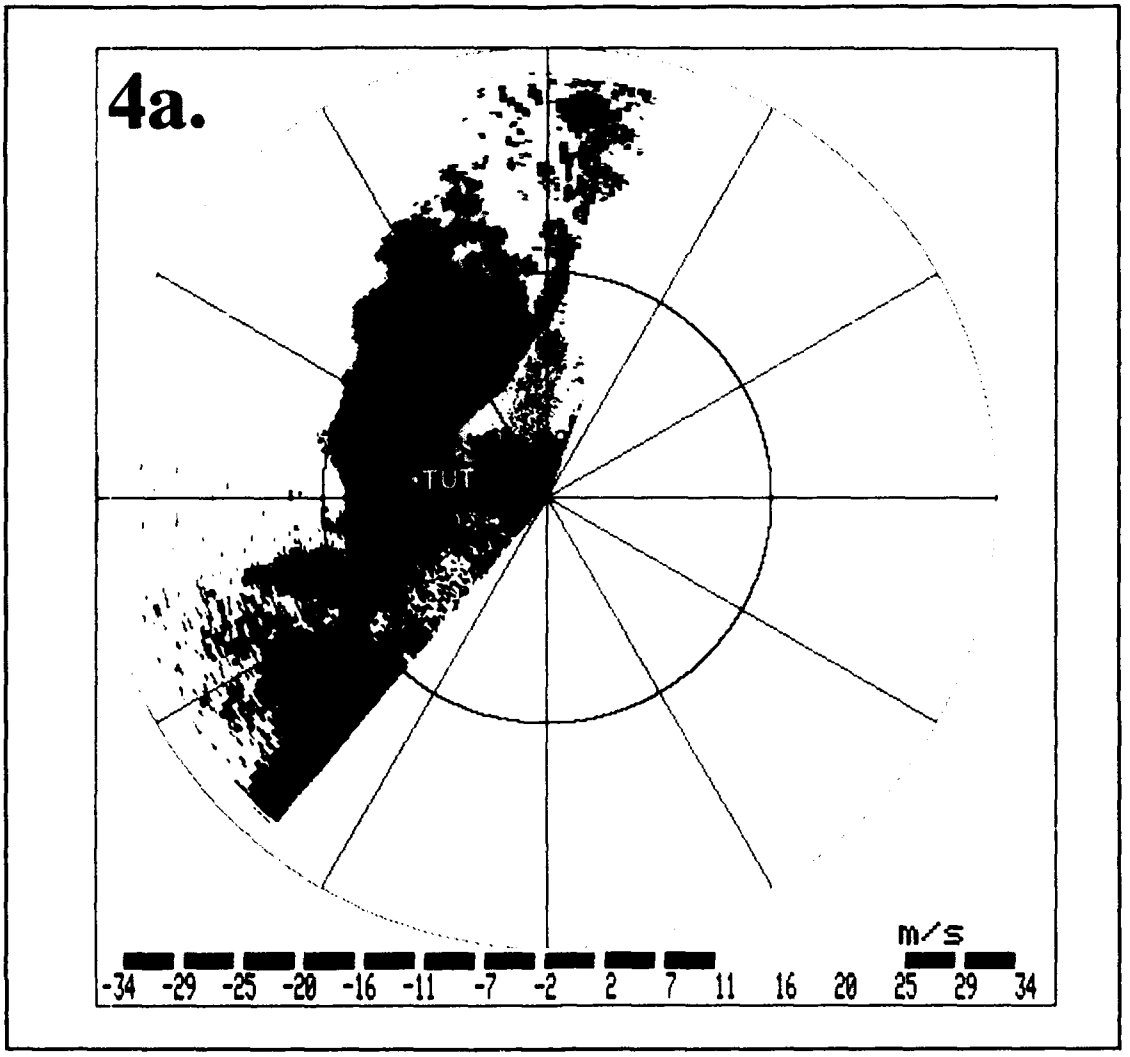

Fig. 4. Same as Fig. 2 except for 0252 UTC. SAM site TUT measured a surface gust front passage within 2 minutes of this scan. SAM location is plotted on Fig. 4a.

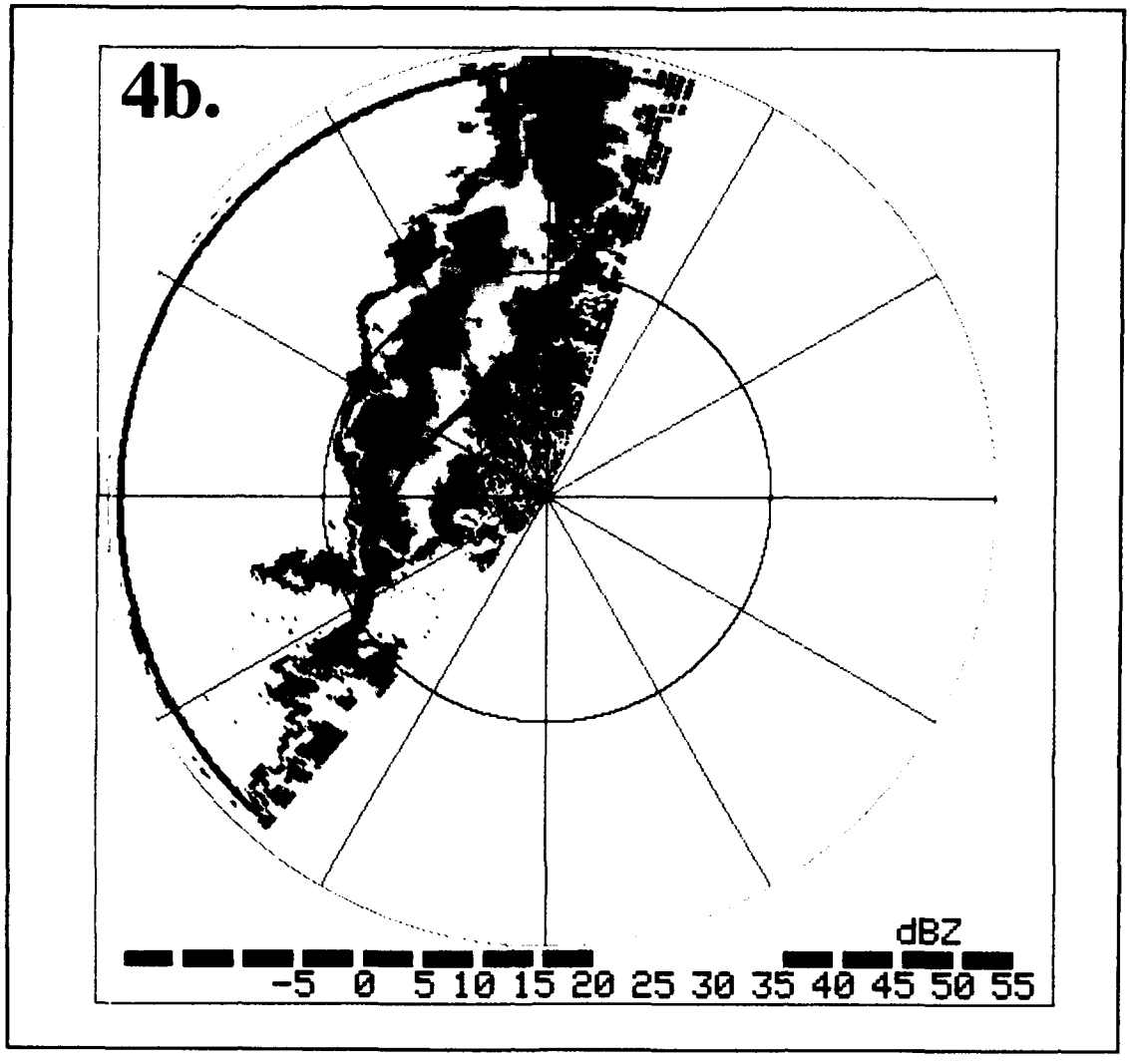

Fig. 4. (continued)

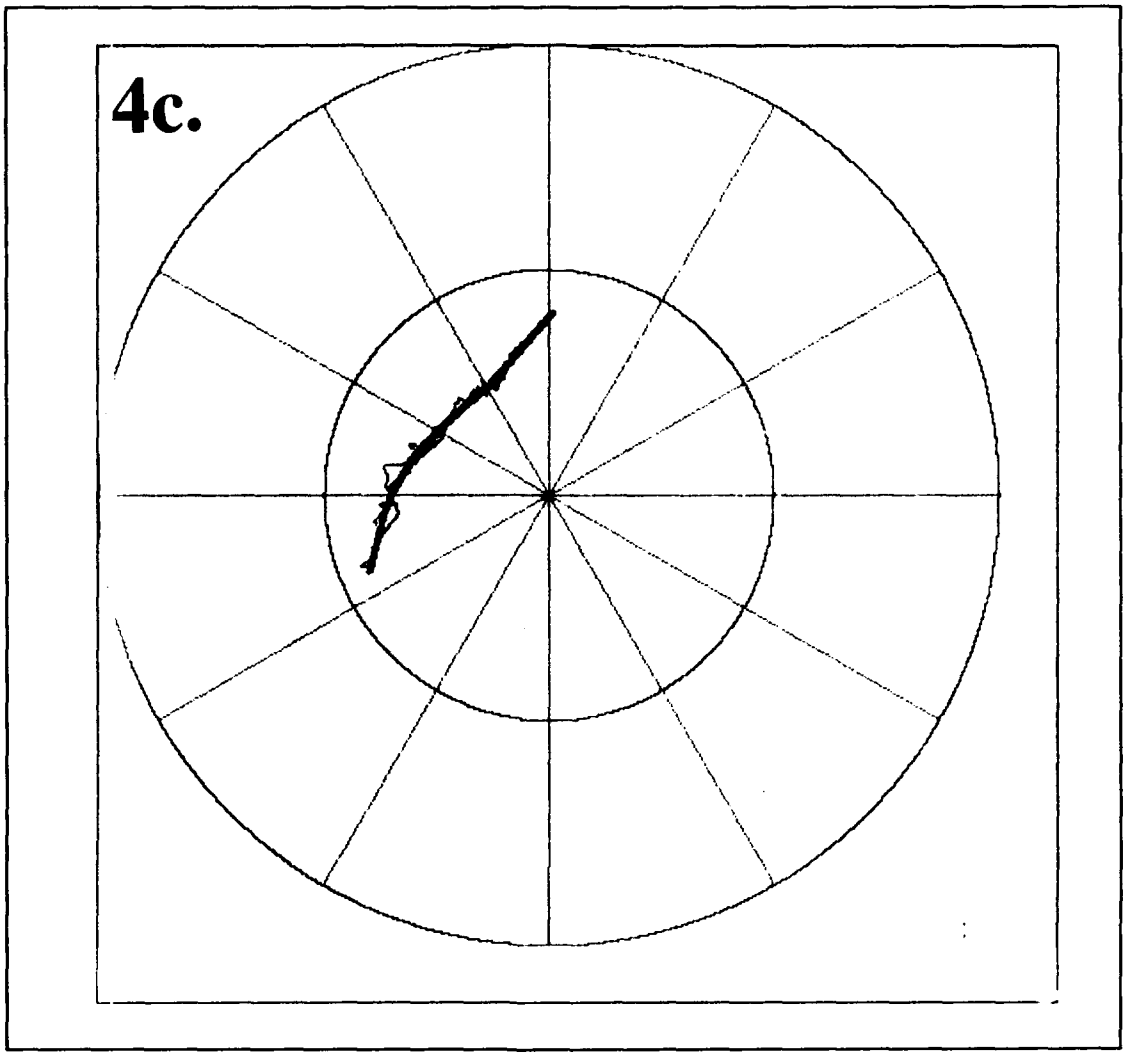

Fig. 4. (continued)

At 0252 UTC, the gust front detection is 33 km from the radar (Fig. 4a). Along the northern half of the gust front, the detection has moved even farther away from the leading edge of the reflectivity gradient (Fig. 4b). Features from both tilts are now roughly on top of each other (Fig. 4c). The SAM station TUT experienced a gust front passage about 3 km ahead of the gust front detection. Again, using Eq. (1), the 0.5° and 1.5° radar beams are determined to be approximately 0.3 km and 1.0 km AGL at the location of the SAM station.

In summary, as this gust front approached the radar: a) the average distance between the upper and lower tilt features comprising the gust front detection decreased; and, b) the distance between the gust front detection and the leading edge of reflectivity gradient increased. Also, at a range of 60 km, the GFDA produced detections at the same time that Surface Automated Mesonet (SAM) stations some 5-7 km ahead of the algorithm detections were reporting wind shifts. Closer to the radar, the SAM detections of the surface wind shift were found only 3 km ahead of the algorithm detections. These observations suggest that the GFDA is detecting the sloped shear zone found aloft behind the surface gust front.

6.3 Grouping and Length Thresholds.

There are other problems with detecting distant fronts. At far ranges, gust fronts must be longer to contain the minimum number of shear segments (five), because spatial resolution between radar azimuths (radials) decreases with increasing range. For example, at a range of 120 km, the distance between 1° radials (the

approximate beam spacing for both radar systems) is just over 2 km (Table 5); at a range of 30 km, this distance is only about 0.5 km. At ranges of 120 km and 60 km, a shear feature containing 5 shear segments would be 8.36 km and 4.18 km long respectively. Beyond a range of 72 km, a shear feature containing 5 shear segments would be greater than 5 km long, the minimum feature length threshold. Therefore, fewer short features will be detected as slant range increases, and subsequently, fewer short gust fronts will be detected.

Table 5. The distance in km between 1° radials versus slant range in km.

DIST FROM RADAR (km)	DIST BETWEEN 1° 1° RADIALS (km)
30	0.52
60	1.05
100	1.75
120	2.09
240	4.19

6.4 Wind Shift Estimates.

Wind speed and direction estimates (Witt et al., 1989) ahead and behind gust fronts will be degraded at far ranges. Turbulence, moisture, and temperature typically decrease with height in the troposphere. These are all factors in determining clear-air echo strength (Doviak and Zrnić, 1984). At distant ranges, the radar beam is higher above the ground, so there is typically less signal return. Also, given the same echo strength, the signal power returned to the radar will decrease as $1/r^2$ (Doviak and Zrnić, 1984) where r = slant range. Therefore, signal-to-noise

ratios decrease by $1/r^2$. These two factors (radar beam height and the $1/r^2$ loss of signal power) contribute to weak signal return at far ranges.

The wind shift estimation technique has several data quality constraints that require a minimum number of radar velocity estimates to approximate wind speed and direction. If a large number of velocity estimates are missing due to poor signal return, speed and direction estimates will not be made. Furthermore, at far ranges the front detections may actually represent a shear zone above and behind the surface gust front (Fig. 1). These wind estimates may be unrepresentative of surface wind conditions.

6.5 Suggestions for detecting distant and shallow gust fronts.

Between the ranges where average gust fronts can be detected on either of the two low-elevation tilts, features from just the lower tilt could be used alone to establish a front detection (i.e., no vertical association). This will increase detectability at distant ranges. To reduce the number of potential false alarms, time association and minimum feature length could be used to discriminate gust front detections. This method could allow for front detections of 2 km deep fronts to a range of 125 km (see Table 3). Unfortunately, this is still about one-half of the 240 km working range of the WSR-88D radar.

7. Conclusions.

The TDWR and WSR-88D radar systems differ in data resolution and tilt sequences. The impacts of these differences will have varying impacts on the performance of the GFDA. Impacts will range from the minimal effects of velocity precision differences, to the somewhat major effects due to sample volume resolution differences and larger upper tilt angle.

If the Gust Front Detection Algorithm is to be used on a WSR-88D system, several modifications will have to be made to take advantage of the different data resolution and tilt sequences used. The method to compute the window size for peak shear calculations could be modified. Also, beyond the maximum detectable range of average gust fronts at the highest of the two low-elevation tilts, the vertical association dependence could be removed and replaced with a time association dependence.

The WSR-88D is designed to operate to a greater range than TDWR. There is a maximum detection range for gust fronts. This is based on the depth of the gust front and the height of the radar beam above the ground at a given distance away from the radar. Unfortunately, the higher second low-elevation tilt angle of the WSR-88D system will reduce this maximum detection range.

Beyond the maximum detection range, gust front detections could still be used with caution to estimate actual surface conditions knowing that: a) the convergence detected is aloft and usually behind the surface gust front; and, b) wind estimates will not always represent surface wind shift conditions. Other meteorological phenomena

can be associated with lines of convergence (Stumpf, 1991), and may be detected by the GFDA. With experience and additional research, proper interpretation of algorithm output at distant ranges by WSR-88D users, in conjunction with other known parameters of the environment in the vicinity of the gust front detections, could lead to reasonable estimates of surface conditions.

8. References.

Campbell, S. D., and M. W. Merritt, 1990: TDWR scan strategy requirements, Revision 1. Massachusetts Institute of Technology/Lincoln Laboratory Project Report ATC-144, Revision 1, 17 pp.

Doviak, R. J., and D. S. Zrnić, 1984: *Doppler Radar and Weather Observations*. Academic Press, 458 pp.

Eilts, M. D., S. H. Olson, G. J. Stumpf, L. G. Hermes, A. Abrevaya, J. Culbert, K. W. Thomas, K. Hondl, and D. Klingle-Wilson, 1991: An advanced gust front detection algorithm for TDWR. *25th Conf. on Radar Meteor.*, Paris, France, June 24-28, Amer. Meteor. Soc., J37-J42.

Heiss, W. H., D. L. McGrew, and D. Sirmans, 1990: NEXRAD: Next generation weather radar (WSR-88D). *Microwave Journal*, **33**, 79-98.

Hermes, L. G., K. W. Thomas, G. S. Stumpf, and M. D. Eilts, 1990: Enhancements to the TDWR Gust Front Algorithm. Federal Aviation Administration Report No. DOT/FAA/NR-91/3, 55 pp.

Mahoney, W. P., 1988: Gust front characteristics and the kinematics associated with interacting thunderstorm outflows. *Mon. Wea. Rev.*, **116**, 1474-1491.

Purdom, J. F. W., 1982: Subjective interpretations of geostationary satellite data for nowcasting. *Nowcasting*, K. Browning, Ed., Academic Press, 149-166.

Stumpf, G. S., 1991: Detecting non- gust front phenomena using the gust front algorithm developed for Terminal Doppler Weather Radar. Submitted as a Federal Aviation Administration report.

U. S. Dept. of Commerce, 1988: Limited production phase next generation weather radar-preliminary technical manual. 50-DMNW-8-00032.

Uyeda, H., and D. S. Zrnić, 1985: Automatic detection of gust fronts. Federal Aviation Administration Report No. DOT/FAA/PM-85/11, 51 pp.

Wakimoto, R. M., 1982: The life cycle of thunderstorm gust fronts as viewed with Doppler radar and rawinsonde data. *Mon. Wea. Rev.*, **110**, 1060-1082.

Wit[t] A., and S. D. Smith, 1987: Development and testing of the gust front algorithm. Federal Aviation Administration Report No. DOT/FAA/PS-87/4, 30 pp.

Witt, A., S. D. Smith, M. D. Eilts, L. G. Hermes, and D. L. Klingle-Wilson, 1989: Gust front/wind shift detection algorithm for the Terminal Doppler Weather Radar. Federal Aviation Administration Report No. DOT/FAA/NR-91/4, 64 pp.